ELSEVIER

Eur. J. Med. Chem. 37 (2002) 111–125

EUROPEAN JOURNAL OF MEDICINAL CHEMISTRY

Original article

CoMFA analysis of the human β_1-adrenoceptor binding affinity of a series of phenoxypropanolamines

Simon N. Louis, Linda A. Rezmann-Vitti, Tracy L. Nero, Dimitri Iakovidis, Graham P. Jackman, William J. Louis *

Department of Medicine, Clinical Pharmacology and Therapeutics Unit, The University of Melbourne, Austin and Repatriation Medical Centre, Heidelberg, 3084 Victoria, Australia

Received 11 April 2001; received in revised form 21 November 2001; accepted 22 November 2001

Abstract

A series of 36 phenoxypropanolamines was examined to determine the structure–activity relationships of β-adrenoceptor (β-AR) antagonists for the human β_1-AR. The binding affinities of all the compounds were determined for human β_1-ARs expressed in Chinese hamster ovary cells and the antagonist potency for rat atrial β_1-ARs was determined for 32 of these compounds for comparative purposes. The compounds, based upon a phenoxypropanolamine core structure with various *meta*-, *ortho*-, *para*- and amine-substituents, displayed binding affinities (pK_i) for the human β_1-AR ranging from 5.49 to 9.35. Antagonist potencies (pA_2) in the rat ranged from 5.52 to 9.56 and correlated with the human binding affinities ($r^2 = 0.86$). Twenty-six compounds were used as the training set for comparative molecular field analysis (CoMFA) of antagonist binding affinity at the human β_1-AR and also of antagonist potency for rat atrial β_1-ARs. The CoMFA models were derived using both the CoMFA electrostatic and steric field parameters. The initial human β_1-AR model ($n = 26$, $q^2 = 0.59$, ONC = 6, $SE_{CV} = 0.70$, $r^2 = 0.98$, $SE_{non\text{-}CV} = 0.16$, $F(6, 19) = 148$) predicted the binding affinities of seven out of ten test compounds, not included in the training set, with residual pK_i values ≤ 0.50. The final human β_1-AR model ($n = 36$, $q^2 = 0.66$, ONC = 5, $SE_{CV} = 0.61$, $r^2 = 0.95$, $SE_{non\text{-}CV} = 0.24$, $F(5, 30) = 107$), consisting of the training set plus the test set of compounds, may prove useful in the design of new phenoxypropanolamine type β_1-AR antagonists. The initial rat β_1-AR model ($n = 26$, $q^2 = 0.42$, ONC = 6, $SE_{CV} = 0.76$, $r^2 = 0.94$, $SE_{non\text{-}CV} = 0.25$, $F(6, 19) = 47$) predicted the affinities of five out of six test compounds with residual pA_2 values ≤ 0.50. The final rat β_1-AR model (i.e. training set plus test set of compounds) ($n = 32$, $q^2 = 0.38$, ONC = 5, $SE_{CV} = 0.69$, $r^2 = 0.93$, $SE_{non\text{-}CV} = 0.24$, $F(5, 26) = 67$) in particular has a low q^2 value, indicating that, at least for the rat, the biologically active phenoxypropanolamine conformation may be quite different to the low energy extended conformation chosen for this CoMFA study. © 2002 Published by Éditions scientifiques et médicales Elsevier SAS.

Keywords: comparative molecular field analysis; human beta1-adrenoceptors; beta-adrenoceptor antagonists; phenoxypropanolamines; quantitative structure–activity relationships

1. Introduction

Drugs (i.e. β-blockers or antagonists) that inhibit the activity of the endogenous catecholamines, noradrenaline and adrenaline, at β-adrenoceptors (β-ARs) are used as treatments for a number of cardiovascular conditions including hypertension, ischaemic heart disease and heart failure [1]. At least three β-AR subtypes exist and these have been cloned and sequenced from the human genome [2–4]. Recently, we have examined

Abbreviations: β-AR, β-adrenoceptor; CoMFA, comparative molecular field analysis; ONC, optimum number of components; PLS, partial least squares; SE_{CV}, cross validated PLS standard error; $SE_{non\text{-}CV}$, non-cross validated PLS standard error; CHO cells, Chinese hamster ovary cells; ICYP, [^{125}I]-(−)-iodocyanopindolol; LOO, leave-one-out; q^2, cross validated r^2; MR, molar refractivity.

* Correspondence and reprints.

E-mail address: ajenkins@austin.unimelb.edu.au (W.J. Louis).

0223-5234/02/$ - see front matter © 2002 Published by Éditions scientifiques et médicales Elsevier SAS.

PII: S0223-5234(01)01315-0

the effects of *para*-substitution upon antagonist potency (pA_2) at the rat β_1-AR and β_2-AR in a series of *N*-isopropylphenoxypropanolamines using comparative molecular field analysis (CoMFA) [5]. In addition to the standard CoMFA electrostatic and steric field parameters, we examined the effects of including a number of other physical characteristics of the compounds, such as log *P*, in our CoMFA analysis. For *para*-substituted *N*-isopropylphenoxypropanolamines it appears at least two factors contribute to potency at the rat β_1-AR. These are the ability of the *para*-substituent to access a bulk preferring pocket and the charge of the phenyl ring [5].

To date most structure–activity studies have relied on animal experimental data. In this study, we have looked at antagonist binding to human β_1-ARs in the belief that this will be more relevant to therapeutic use. To do this we have examined the binding affinities of 36 compounds for human β_1-ARs expressed in Chinese hamster ovary (CHO) cells and the structure–activity relationships, determined using CoMFA analysis. In contrast to the previous study where we only examined the effect of *para*-substitution, in the present study we have also looked at the effect on binding affinity at human β_1-ARs and potency at rat β_1-ARs of various *ortho*-, *meta*-, *para*- and amine-substitutions of a phenoxypropanolamine core structure. In addition, we have examined differences between the human and the rat β_1-AR by comparing the human binding data with the antagonist potency for atrial rat β_1-ARs for 32 of these compounds.

2. Chemistry

The synthetic routes for all of the compounds (Tables 1 and 2) have been previously reported and they were prepared as their racemic mixtures by the general procedure shown in Fig. 1. For simplicity, all of the compounds will be referred to by the numbers given in Tables 1 and 2, this includes the following well known compounds; atenolol (**2**), practolol (**3**), metoprolol (**4**), betaxolol (**6**), H87/07 (**7**), cicloprolol (**8**), RO 31-1118 (**9**), propranolol (**10**), ICI-118,551 (**11**), bupranolol (**12**), CGP 12177 (**13**), CGP 20712A (**24**) and LK 204-545 (**26**). It has been established for simple phenoxypropanolamines that the *S*-isomer is the active isomer, with little β-AR activity residing with the *R*-isomer [6–8]. Resolution of the racemate into the individual isomers or stereospecific synthesis was therefore not carried out.

The appropriate phenols **A** reacted under aqueous alkaline conditions with epichlorohydrin to produce the epoxides **B** (Fig. 1). After isolation the crude epoxides **B** were used without further purification. The *N*-isopropyl compounds **1**–**6**, **8**, **9**, **27** and **28** were prepared by the overnight reaction of the corresponding epoxides **B** with excess isopropylamine and were purified by chromatography on silica gel [5]. Compound **12** was prepared by the reaction of the corresponding epoxide **B** with excess *t*-butylamine and then purified in a similar manner to the *N*-isopropyl compounds [9].

Compounds **14**–**19**, **21**–**23**, **29**–**35** [10] were prepared by the reaction of the corresponding epoxides **B** with ethylene diamine-4-tetrahydropyrancarboxylic acid monoamide in dioxane at reflux for 6 h and the reaction mixtures were purified on silica gel [10]. The synthesis of ethylene diamine-4-tetrahydropyrancarboxylic acid monoamide has been previously described [10]. Compound **20** was prepared in a similar manner using the corresponding ketal monoamide (Fig. 2), the synthesis of which has also been previously described [10]. Compounds **25** [11], **26** [12] and **36** [13] were prepared by the reported procedures.

The physical and chemical data for all intermediates and final products were in agreement with the previously reported values. Compounds **7** (H87/07), **10** (propranolol), **11** (ICI-118,551), **13** (CGP 12177) and **24** (CGP 20712A) were purchased directly from the relevant companies (refer to Section 7.1).

3. Pharmacology

The ability of the compounds to inhibit specific [^{125}I]-(−)-iodocyanopindolol (ICYP) binding to human β_1-ARs expressed in CHO cells was examined, as were the dissociation constants (K_d) and maximal density of binding sites (B_{max}) of ICYP for the transfected human β_1-AR. Binding data were analysed using the iterative curve fitting programs EBDA Version 4.0 which incorporates LIGAND Version 4.0 [14,15]. The log of the inhibition constants (pK_i) (drug inhibition studies) are shown as mean ± S.E.M. ($n = 3$–4) in Tables 1 and 2. Pseudo Hill coefficients (n_H) were obtained from the binding data using the sigmoidal fit of the EBDA program.

Functional antagonist potency of the rat β_1-AR was assessed by the ability to inhibit the chronotropic effects of (−)-isoprenaline on isolated rat atria (pA_2) and reported in Tables 1 and 2. We had previously determined the pA_2 values for 17 of these compounds (**1**–**13**, **24** and **26**–**28**) [5,16] and in this study, we have evaluated the pA_2 values for a further 15 compounds (**14**–**23**, **25**, **30** and **32**–**34**) (there was an insufficient amount of compounds **29**, **31**, **35** and **36** for the pA_2 values to be determined). Cumulative concentration–response curves were obtained in each preparation as described by Van Rossum et al. [17] and curves were fitted by computer analysis according to the method of Zabrowsky et al. [18] using the sigmoidal fit function of the Origin graphics package (MicroCal Origin, MicroCal Software Inc., One Roundhouse Plaza, Northamp-

Table 1
Binding affinities (pK_i) for human β_1-ARs, antagonist potencies (pA_2) for rat β_1-ARs, molar refractivities (MR) and log P values for the compounds in the training set ($n = 26$)

No.	Structure	Human β_1-AR pK_i[a]	Rat β_1-AR pA_2[b]	MR[c]	$LogP$[d]
1	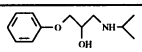	8.42 ± 0.10	8.09± 0.14	61.1	1.76
2	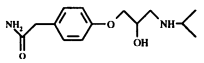	6.88 ± 0.11	7.30 ± 0.12	74.3	0.44
3	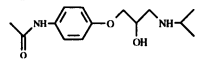	6.78 ± 0.05	6.85 ± 0.06	75.4	0.78
4	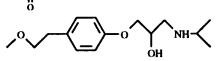	7.65 ± 0.13	7.60 ± 0.17	77.1	1.87
5	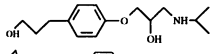	7.07 ± 0.14	7.13 ± 0.10	76.9	1.82
6	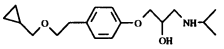	8.75 ± 0.11	8.06 ± 0.15	88.9	2.72
7	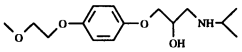	7.00 ± 0.01	7.37 ± 0.09	78.8	1.63
8	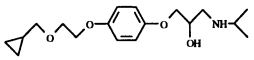	7.97 ± 0.03	7.73 ± 0.07	90.7	2.48
9	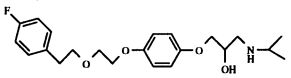	8.82 ± 0.06	7.98 ± 0.21	107.9	3.81
10	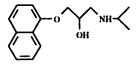	8.89 ± 0.11	8.40 ± 0.32	79.0	3.00
11	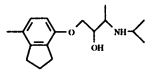	7.38 ± 0.06	6.92 ± 0.13	82.7	3.67
12	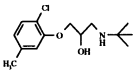	9.04 ± 0.10	9.30 ± 0.15	75.5	3.12
13	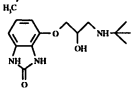	9.35 ± 0.28	9.56 ± 0.18	75.6	0.76
14	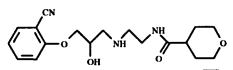	8.08 ± 0.19	7.43 ± 0.16	92.6	-0.14
15	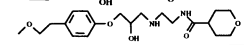	7.00 ± 0.07	7.11 ± 0.22	103.3	0.14
16	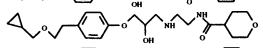	7.61 ± 0.06	7.35 ± 0.11	115.1	0.97
17	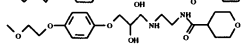	5.87 ± 0.06	6.04 ± 0.10	105.0	-0.26
18	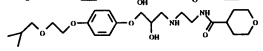	7.40 ± 0.10	7.81 ± 0.18	118.9	1.01
19	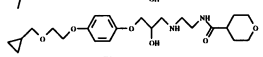	6.75 ± 0.15	7.00 ± 0.06	116.9	0.57
20	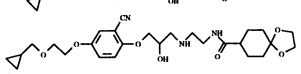	7.51 ± 0.09	7.53 ± 0.07	135.4	1.05
21	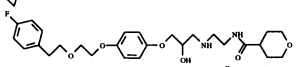	8.02 ± 0.10	7.80 ± 0.21	134.1	1.96
22	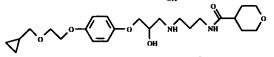	5.49 ± 0.10	5.52 ± 0.40	121.5	0.93
23	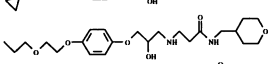	7.31 ± 0.12	7.21 ± 0.07	119.1	1.04
24	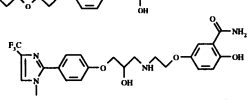	8.48 ± 0.19	8.52 ± 0.15	118.2	2.90
25	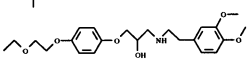	7.92 ± 0.01	7.72 ± 0.11	116.7	3.00
26	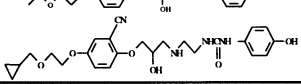	8.52 ± 0.12	8.53 ± 0.08	128.9	2.65

[a] pK_i is the binding affinity and expressed as mean ± s.e.m. of 3-4 individual experiments. [b] pA_2 is the antagonist potency and expressed as mean ± s.e.m. of 4-9 individual experiments. [c] MR is the molar refractivity of the compound calculated using ACD/Chem Sketch.
[d] $LogP$ is the $logP$ calculated using PrologP.

Table 2
Binding affinities (pK_i) for human β_1-ARs, antagonist potencies (pA_2) for rat β_1-ARs, molar refractivities (MR) and log *P* values for the compounds in the test set

No.	Structure	Human β_1-AR pK_i[a]	Rat β_1-AR pA_2[b]	MR^c	$LogP^d$
27	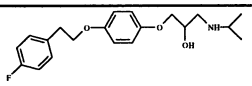	8.71 ± 0.03	8.01 ± 0.12	96.9	3.95
28	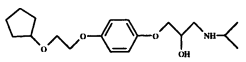	8.60 ± 0.14	8.04 ± 0.30	95.2	3.13
29	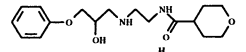	7.57± 0.16	ND[e]	87.3	-0.05
30	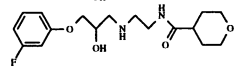	7.53 ± 0.26	7.32 ± 0.09	87.3	0.21
31	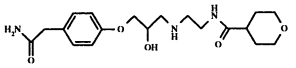	5.81 ± 0.10	ND	100.4	-1.39
32	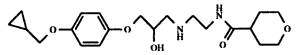	6.80 ± 0.08	6.97 ± 0.14	105.9	0.74
33	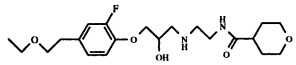	6.85 ± 0.07	7.25 ± 0.09	107.9	0.28
34	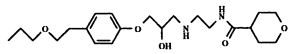	7.90 ± 0.22	7.20 ± 0.09	112.5	1.11
35	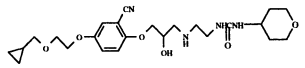	6.97± 0.05	ND	125.5	0.62
36	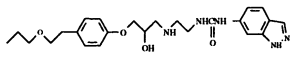	9.07± 0.08	ND	129.5	3.16

[a,b,c,d]as defined in *table I*. [e]ND, no data.

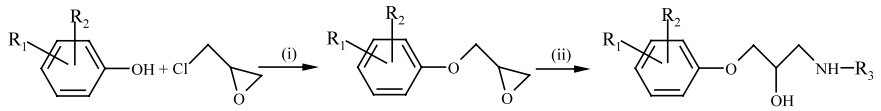

A B C

Fig. 1. General procedure for preparing *N*-alkylphenoxypropanolamines. Reagents: (i) aqueous KOH, EtOH; (ii) alkylamine (R_3NH_2), EtOH.

ton, MA 01060, USA). The pA_2 values represent the mean ± S.E.M. from 4 to 9 individual experiments.

4. Molecular modelling and QSAR analysis

4.1. Molecular modelling, conformer selection and alignment

Modelling studies were performed using the SYBYL software package (Tripos Inc., 1699 S. Hanley Rd, St. Louis, MO 63144-2913, USA, version 6.6) on a Silicon Graphics Indigo 2 unix workstation. The structure of the active *S*-isomer of compound **1** (Table 1) was constructed from standard bond lengths and bond angles using the sketch routine in SYBYL. The geometry of compound **1** was fully optimised in vacuo as previous studies [8] have identified that the propanolamine side-chain of aryloxypropanolamine compounds can adopt common conformations in solid, theoretical gas and solution states. The phenoxypropanolamines are inherently flexible molecules, and the active receptor bound conformation(s) is unclear. However, docking studies using our model of the human β_1-AR [19] indicate that an extended antagonist conformation is able to dock into the receptor active-site and satisfy all of the known interactions with the β_1-AR. Hence, as a starting point we have chosen low energy extended conformers of the phenoxypropanolamines for this CoMFA study. In our previous CoMFA study on *N*-isopropylphenoxy-

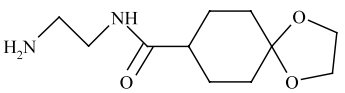

Fig. 2. Ketal monoamide used in the synthesis of compound **20**.

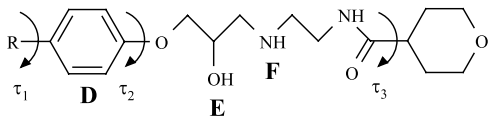

Fig. 3. Structure of compound **29** (where R = H). The torsion angles τ_1 and τ_2 define the conformation of the *para*-substituent (R) and the oxypropanolamine side-chains, respectively in relation to the phenyl ring, for example when $\tau_1 = 0$ the *para*-substituent is planar to the phenyl ring. The torsion angle τ_3 defines the conformation of the tetrahydropyran ring of compounds **14**–**19**, **21**–**23** and **29**–**35**. The phenoxypropanolamine type compounds are thought to interact with the β-AR via a three point pharmacophore consisting of the phenyl ring (**D**), the β-hydroxyl group (**E**) and the amino group (**F**).

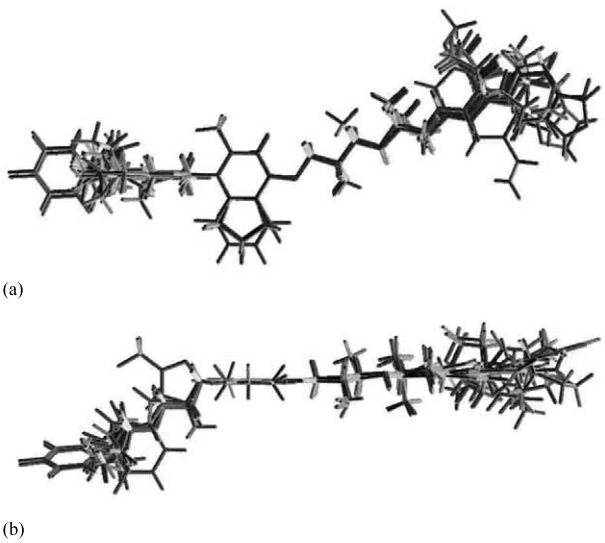

Fig. 4. Superimposition via the β-hydroxyl oxygen atom (**E**), the amino group nitrogen atom (**F**) and the phenyl ring (**D**) of the 26 compounds used in the training set: (a) view from above the phenyl ring; and (b) side view (i.e. 90° rotation around the *x*-axis from view (a)).

propanolamines in the rat [5] we determined that the cross validated r^2 (q^2) was maximised when $\tau_1 = 90$ and $\tau_2 = 0°$ (Fig. 3), therefore in the present study we have constructed the compounds using these torsion angle values. These values for τ_1 and τ_2 are consistent with previous pharmacophore modelling studies carried out by us and others [[8,20,21] and references contained within]. Optimisation was conducted using the AM1 Hamiltonian in MOPAC (version 6.0) [22], the keywords 'PRECISE' and 'NOMM' were specified.

The *N*-isopropyl compounds **2**–**11**, **27** and **28** (Tables 1 and 2) were constructed using the minimised structure of compound **1** as a starting point. Compound **11** has two chiral centres and the active (*S*,*R*) diastereomer is the one used here. The appropriate substituents were added in an extended conformation. The structures were then optimised using the AM1 Hamiltonian in MOPAC, with the keywords 'PRECISE' and 'NOMM' specified, however τ_1 and τ_2 were fixed at 90 and 0°, respectively (Fig. 3) and the bond, dihedral and valence angles of the phenoxypropanolamine core structure were fixed at the optimised values for compound **1**. The *N*-*t*-butyl compounds **12** and **13** were also constructed using compound **1** as a starting point and then modifying the amine-substituent and phenyl ring substituents as necessary. The structures of **12** and **13** were then optimised as described above. Similarly, the amine-substituent of compound **29** (Table 2) was added to the minimised structure of compound **1** and the entire structure was optimised as above. In addition, τ_3 (Fig. 3) was varied independently (i.e. the tetrahydropyran ring was rotated while the rest of the molecule was fixed) in 30° steps through a full 360°, giving a total of 12 conformations and the heat of formation was calculated for each conformer. The AM1 heat of formation was lowest when $\tau_3 = 300°$ ($\Delta H_f = -160.0$ kcal mol^{-1}) and highest when $\tau_3 = 60°$ ($\Delta H_f = -150.01$ kcal mol^{-1}), therefore, τ_3 was set to 300° for compound **29**. Compounds **14**–**26** and **30**–**36** (Tables 1 and 2) were then constructed using the minimised structure of compound **29** as a starting point, making structural modifications as required, and optimised as described above.

The alignment of the compounds is a very important feature of CoMFA analysis [23]. It has been proposed that aryloxypropanolamine type compounds interact with β-ARs via a three point pharmacophore consisting of the β-hydroxyl group, the amino group and an electron rich moiety which is usually a phenyl ring (features **E**, **F** and **D**, respectively in Fig. 3) [24,25] and more recent site-directed mutagenesis studies support this hypothesis [21,26–28]. If we assume the compounds all act via the same mechanisms, then these common points of interaction must superimpose and for simplicity we have assumed that the phenoxypropanolamine core structure remains fixed for all compounds in our alignment (Fig. 4) [5].

Compound **1** was used as the template and all of the compounds were superimposed onto compound **1** via the three common interaction points; the phenyl ring (**D**), the β-hydroxyl oxygen atom (**E**) and the amine nitrogen atom (**F**) (Figs. 3 and 4) using the Fit Atoms root mean square routine within SYBYL.

4.2. Log P calculations

The log *P* values for the 36 compounds (Tables 1 and 2) were calculated using the PALLAS PROLOGP (CompuDrug International Inc., 705 Grandview Drive, Sth San Francisco, CA 94080, USA, version 1.1) program.

4.3. Molar refractivity calculations

The molar refractivity (MR) values for the 36 compounds (Tables 1 and 2) were calculated using the program ACD/CHEM Sketch (Advanced Chemistry

Development Inc., 90 Adelaide St. West, Toronto, Ontario, Canada M5H 3V9, version 4.55).

4.4. Development of the CoMFA model

CoMFA [23] was performed using the QSAR option in SYBYL for the 26 compounds in the training set for both the human and rat β_1-AR data (Table 1). Both steric and electrostatic fields were considered. The electrostatic CoMFA fields were calculated using MOPAC AM1 charges. The probe atom had the properties of an sp^3 carbon atom and a charge of $+1.0$. Cut-off values were SYBYL default values, a distance-dependent dielectric constant was used and the grid step size was 2.0 Å. All other parameters were set to the SYBYL default settings. The effects of changing column filtering values (1.0–7.0 kcal mol^{-1}) were examined. Column filtering omits from the analysis columns (lattice points) whose variance is less than the specified value. The CoMFA QSAR equations were generated using the partial least squares (PLS) algorithm and the leave-one-out (LOO) cross validation procedure. The number of components with the lowest standard error (SE_{CV}) of prediction value and highest q^2 was selected as the optimum number of components (ONC). As the training set of compounds is relatively small ($n = 26$) the ONC was also restricted to seven or below in an attempt to avoid over-fitted models. To further confirm the selection of the ONC and validity of the CoMFA models, we experimented with leaving 2, 3, 4, and 5 compounds out of the training set in random groups. In each case the ONC was found to be the same as that obtained by the LOO cross validation procedure, hence only the data for the LOO cross validation procedure is reported here. The additional physical parameters log P and MR were also included in the cross validated PLS analysis but were found to provide no additional statistical improvements.

5. Results

5.1. Radioligand binding studies

The dissociation constant ($K_d = 4.99 \pm 0.48$ pM) and density of binding sites ($B_{max} = 1523 \pm 295$ fmol mg protein^{-1}) of ICYP for the transfected human β_1-ARs were determined by saturation binding experiments [16,29]. Inhibition binding studies were used to determine the binding affinities of the compounds for the human β_1-ARs. The pK_is of the compounds for displacing ICYP binding from the human β_1-AR are given in Tables 1 and 2 and ranged from 5.49 to 9.35. As expected, saturation binding and displacement curves were consistent with a single binding site population (Hill Slopes, $n_H \cong 1.0$). Compounds **12** (bupranolol), **13** (CGP12177) and **36** displayed the highest affinities for human β_1-ARs (pK_is ≥ 9), whereas compounds **17**, **22** and **31** displayed the lowest (pK_is ≤ 6).

5.2. Isolated rat atria

Functional potencies (pA_2s) for 32 of the compounds at inhibiting (−)-isoprenaline-induced β_1-AR mediated chronotropic effects in spontaneously beating rat atria are listed in Tables 1 and 2 and ranged from 5.52 to 9.56. In agreement with the binding studies, compounds **12** (bupranolol) and **13** (CGP12177) were the most potent antagonists at rat β_1-ARs (pA_2s ≥ 9), whereas compounds **17** and **22** displayed the lowest potencies (pA_2s ≤ 6).

5.3. Comparison of human and rat β_1-AR pharmacological data

There was a reasonable correlation between the pK_is for human β_1-ARs and pA_2s for rat β_1-ARs for the 32 compounds for which we have data (rat $\beta_1 - pA_2 = 1.28 + 0.82 \times$ human $\beta_1 - pK_i$, $r^2 = 0.86$ Fig. 5).

5.4. CoMFA analysis for antagonist binding affinity at the human β_1-AR

The results of the CoMFA cross validated PLS analyses of the binding affinities at the human β_1-ARs of the 26 compounds in the training set are given in Table 3. Cross validated PLS analysis of the data identified that when the default CoMFA settings were used, which included both steric and electrostatic fields, the highest q^2 value was obtained when column filtering was set to 3.0 kcal mol^{-1} ($q^2 = 0.59$, ONC = 6, $SE_{CV} = 0.70$; Table 3). In addition to the CoMFA electrostatic and steric fields, two other physical parameters of the compounds were determined and included in further PLS analysis. These parameters were log P, to introduce a lipophilic field, and MR, which is related to molar volume and London dispersion forces (Tables 1 and 2). Neither log P nor MR offered any statistical benefit over the CoMFA fields alone (Table 3).

Our initial CoMFA model for the human β_1-AR ($n = 26$) was obtained using the CoMFA electrostatic and steric fields, six ONC and 3.0 kcal mol^{-1} column filtering and had the non-cross validated PLS statistics of $r^2 = 0.98$, $SE_{non\text{-}CV} = 0.16$, $F(6, 19)$ of 148. The relative contributions of the CoMFA field components were: steric, 0.48; and electrostatic, 0.52. Fig. 6*a* displays the relationship between predicted and experimental affinities for the non-cross validated analysis, and the residual values are given in Table 4.

The initial human β_1-AR CoMFA model predicted seven out of ten test compounds with residual values ≤ 0.50 (Table 5, Fig. 6b). The model underestimated

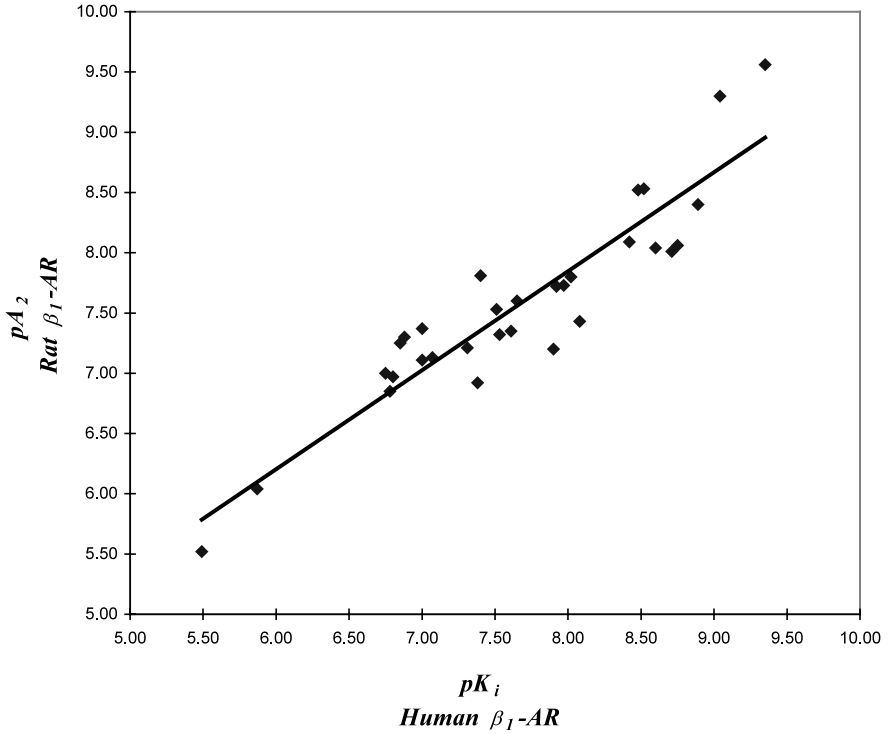

Fig. 5. Plot of the pK_i values for human β_1-ARs transfected into CHO cells verses the pA_2 values for rat β_1-ARs in isolated rat atria.

the affinity of compounds **27**, **28** and **32** (Table 5, Fig. 6b).

The final human β_1-AR CoMFA model was constructed using the compounds in both the training and the test sets ($n = 36$). In these analyses column filtering was also set to 3.0 kcal mol^{-1} as this produced the highest q^2. The cross validated PLS statistics were; ONC = 5, $q^2 = 0.66$ and $SE_{CV} = 0.61$. The non-cross validated statistics for the model were: $r^2 = 0.95$, $SE_{non\text{-}CV} = 0.24$ and $F(5, 30) = 107$. The relative contributions of the CoMFA field components were: steric, 0.45; and electrostatic, 0.55.

5.5. CoMFA analysis for antagonist potency at the rat β_1-AR

The results of the CoMFA cross validated PLS analyses of the antagonist potency at the rat β_1-AR for the training set of compounds ($n = 26$) are given in Table 3. In these analyses column filtering was set to 4.0 kcal mol^{-1} as this maximised q^2. The initial rat β_1-AR CoMFA model included only the CoMFA electrostatic and steric fields (ONC = 6, $q^2 = 0.42$, $SE_{CV} = 0.76$, $r^2 = 0.94$, $SE_{non\text{-}CV} = 0.25$, $F(6, 19) = 47$) and the relative contributions of the CoMFA field components were: steric, 0.47 and electrostatic, 0.53. Fig. 7*a* displays the relationship between predicted and experimental potencies for the non-cross validated analysis and the residual values are given in Table 6.

The initial rat β_1-AR CoMFA model predicted five out of six test compounds with residual values ≤ 0.50 (Table 7, Fig. 7b). The model significantly underestimated the potency of compound **32** (Table 7, Fig. 7b).

The final rat β_1-AR CoMFA model was constructed using the training and test sets combined ($n = 32$). Column filtering was set to 2.0 kcal mol^{-1} as this

Table 3
Human and rat β_1-AR CoMFA cross validated PLS results for the compounds in the training set ($n = 26$)

Analysis variables [a]	Column filtering [b]	q^2 [c]	ONC [d]	SE_{CV} [e]
Human				
CoMFA	**3**	**0.59**	**6**	**0.70**
CoMFA, log *P*	3	0.48	7	0.81
CoMFA, MR	3	0.57	6	0.72
CoMFA, log *P*, MR	3	0.45	7	0.84
Rat				
CoMFA	**4**	**0.42**	**6**	**0.76**
CoMFA, log *P*	4	0.20	7	0.91
CoMFA, MR	4	0.40	5	0.75
CoMFA, log *P*, MR	4	0.17	7	0.93

Bold indicates the options used for the initial model.

[a] The variables log *P* and MR listed in the column have all been defined in Table 1. CoMFA refers to both the steric and electrostatic CoMFA fields.

[b] Column filtering value used in kcal mol^{-1}.

[c] q^2 is the highest cross validated r^2 value.

[d] ONC is the optimum number of components.

[e] SE_{CV} is the standard error for the cross validated PLS analysis.

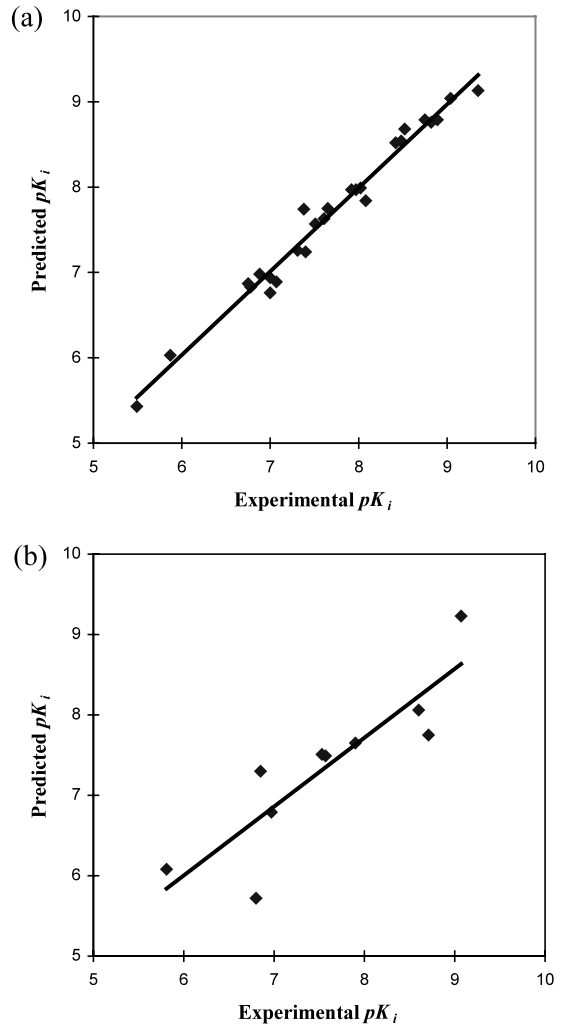

Fig. 6. Plot of the human β_1-AR experimental pK_i values versus the predicted pK_i values for the compounds in: (**a**) the training set, Table 4 ($n = 26$); and (**b**) the test set, Table 5 ($n = 10$).

maximised q^2. The cross validated PLS statistics were; ONC = 5, $q^2 = 0.38$ and $SE_{CV} = 0.69$. The non-cross validated statistics for the model were: $r^2 = 0.93$, $SE_{non\text{-}CV} = 0.24$ and $F(5, 26) = 67$. The relative contributions of the CoMFA field components were: steric, 0.43 and electrostatic, 0.57.

5.6. CoMFA contour maps

The CoMFA contour maps for the final human and rat β_1-AR models are shown in Figs. 8 and 9. The maps were obtained using the PLS analysis standard deviation coefficients, contouring by their contribution and displaying in transparent contour mode. Regions where steric bulk is favoured are depicted in green while yellow indicates where steric bulk is disfavoured. Blue regions depict areas where positive electrostatic charge is favoured and red regions where negative electrostatic charge is favoured.

Fig. 8 shows compound **26** binding within the steric and electrostatic contours for the final human β_1-AR CoMFA model. The experimental data suggests that *para*- and amine-substitution initially decreases antagonist binding affinity at β_1-ARs, e.g. compare compounds **1** and **3** and compounds **1** and **29**. However, it is possible to restore binding affinity by optimising the amine- and *para*-substituents. The human β_1-AR contour map has a region of space where increasing substituent bulk close to the *para*-position of the phenyl ring reduces binding affinity (yellow regions at left hand end of Fig. 8) and a bulk preferring pocket (green

Table 4
Experimental and predicted binding affinities for the training set of compounds ($n = 26$) for human β_1-ARs and the associated residuals

Compound	Experimental pK_i	Predicted pK_i	Residual
1	8.42	8.52	−0.10
2	6.88	6.98	−0.10
3	6.78	6.83	−0.05
4	7.65	7.75	−0.10
5	7.07	6.89	0.18
6	8.75	8.79	−0.04
7	7.00	6.76	0.24
8	7.97	7.97	0.00
9	8.82	8.76	0.06
10	8.89	8.79	0.10
11	7.38	7.74	−0.36
12	9.04	9.04	0.00
13	9.35	9.13	0.22
14	8.08	7.84	0.24
15	7.00	6.94	0.06
16	7.61	7.63	−0.02
17	5.87	6.03	−0.16
18	7.40	7.24	0.16
19	6.75	6.87	−0.12
20	7.51	7.57	−0.06
21	8.02	7.99	0.03
22	5.49	5.43	0.06
23	7.31	7.26	0.05
24	8.48	8.54	−0.06
25	7.92	7.97	−0.05
26	8.52	8.68	−0.16

Table 5
Experimental and predicted binding affinities for the test set of compounds ($n = 10$) for human β_1-ARs and the associated residuals

Compound	Experimental pK_i	Predicted pK_i	Residual
27	8.71	7.75	0.96
28	8.60	8.06	0.54
29	7.57	7.49	0.08
30	7.53	7.51	0.02
31	5.81	6.08	−0.27
32	6.80	5.72	1.08
33	6.85	7.30	−0.45
34	7.90	7.65	0.25
35	6.97	6.79	0.18
36	9.07	9.23	−0.16

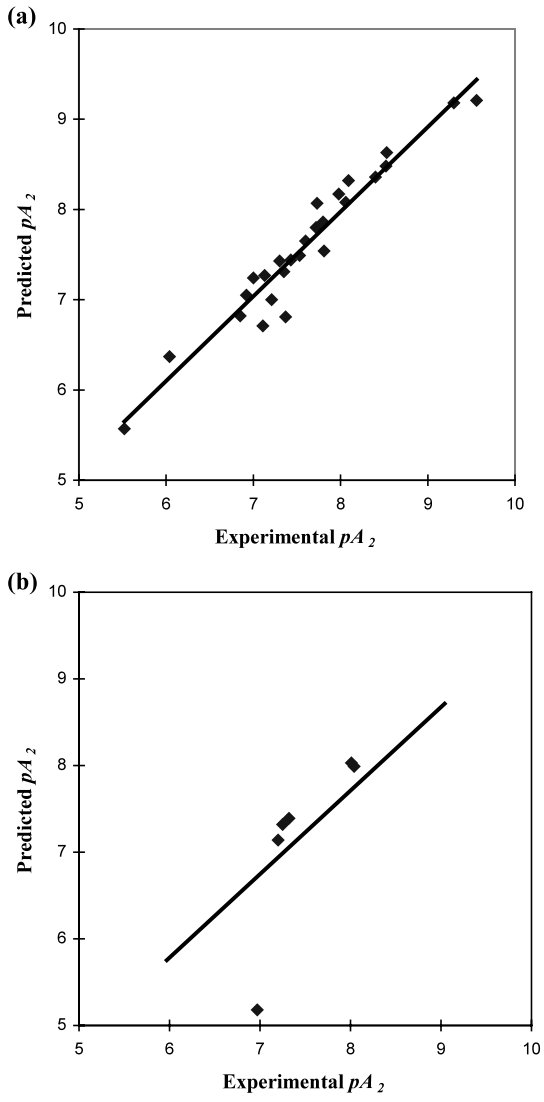

Fig. 7. Plot of the rat β_1-AR experimental pA_2 values verses the predicted pA_2 values for the compounds in: (**a**) the training set, Table 6 ($n = 26$); and (**b**) the test set, Table 7 ($n = 6$).

region) a little further out from this position. Long *para*-substituents, for e.g. compounds **6**, **8**, **9**, **27** and **28** are able to access the bulk preferring pocket leading to a higher binding affinity for the human β_1-AR than those *N*-isopropylphenoxypropanolamines with a shorter *para*-substituent (e.g. compounds **2**, **3** and **5**). Similarly, the map has another bulk preferring region (green region) close to the amine-substituent, suggesting a preference for compounds ending in a *t*-butyl over an *iso*-propyl group or compounds with an amine-substituent containing an α-alkyl group. The CoMFA contour map also has regions which prefer a negative electrostatic charge (shown in red), these regions at the left hand end of Fig. 8 are close to many of the *para*-substituent oxygen atoms, for e.g. compounds **2**, **5**, **17**, **23**, **26** and **35**. The negative electrostatic charge preferring regions, at both ends of Fig. 8, have a positive electrostatic charge preferring core (i.e. blue region located within the red region). The positive electrostatic charge region at the left hand end of Fig. 8 is able to accommodate the *para*-substituent amide functional group of compounds **2** and **31**. The negative electrostatic charge preferring regions (red) at the right hand end of Fig. 8 are close to the ring oxygen atom for many of the tetrahydropyran compounds, for e.g. compounds **15**, **17**, **21**, **30** and **35** and also to the amide oxygen atom. In addition, one of the hydrogen atoms located on the carbon adjacent to the tetrahydropyran ring oxygen atom interacts with the positive electrostatic charge preferring region at the right hand end of Fig. 8. Negative steric interactions (yellow regions) are also important towards the end of the amine-

Table 6
Experimental and predicted potencies for the training set of compounds ($n = 26$) for rat β_1-ARs and the associated residuals

Compound	Experimental pA_2	Predicted pA_2	Residual
1	8.09	8.32	−0.23
2	7.30	7.43	−0.13
3	6.85	6.82	0.03
4	7.60	7.65	−0.05
5	7.13	7.27	−0.14
6	8.06	8.08	−0.02
7	7.37	6.81	0.56
8	7.73	8.07	−0.34
9	7.98	8.17	−0.19
10	8.40	8.36	0.04
11	6.92	7.05	−0.13
12	9.30	9.18	0.12
13	9.56	9.21	0.35
14	7.43	7.44	−0.01
15	7.11	6.71	0.40
16	7.35	7.31	0.04
17	6.04	6.37	−0.33
18	7.81	7.54	0.27
19	7.00	7.24	−0.24
20	7.53	7.49	0.04
21	7.80	7.86	−0.06
22	5.52	5.57	−0.05
23	7.21	7.00	0.21
24	8.52	8.48	0.04
25	7.72	7.80	−0.08
26	8.53	8.63	−0.10

Table 7
Experimental and predicted potencies for the test set of compounds ($n = 6$) for rat β_1-ARs and the associated residuals

Compound	Experimental pA_2	Predicted pA_2	Residual
27	8.01	8.03	−0.02
28	8.04	7.99	0.05
30	7.32	7.39	−0.07
32	6.97	5.18	1.79
33	7.25	7.32	−0.07
34	7.20	7.14	0.06

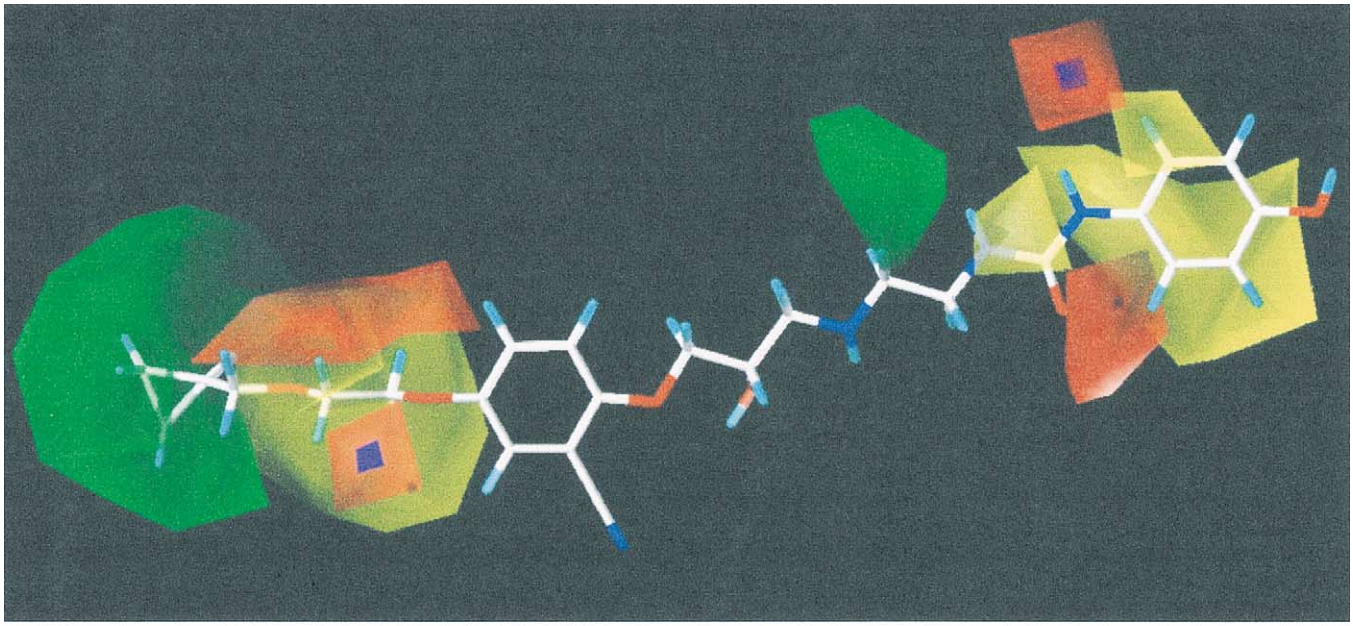

(a)

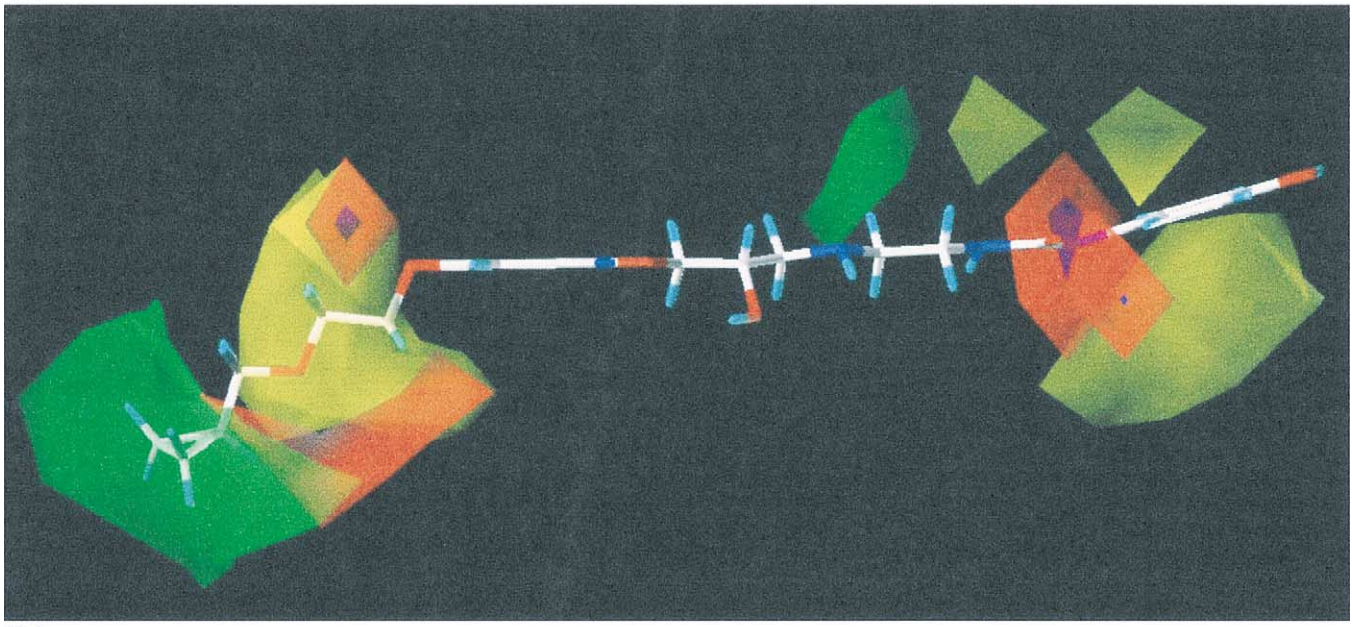

(b)

Fig. 8. Contour map of the final human β_1-AR CoMFA model ($n = 36$) with compound **26** embedded, generated using the CoMFA steric and electrostatic fields. Green regions show favoured areas where increasing bulk is associated with higher binding affinity, yellow regions where increasing bulk is associated with lower binding affinity, blue regions where positive electrostatic charge is associated with higher binding affinity and red regions where negative electrostatic charge is associated with higher binding affinity: (a) view from above the phenyl ring; (b) side view (i.e. 90° rotation about the x-axis from view (a)). Transparent contours were drawn at the 70/30 level, all other 'view CoMFA' parameters were the default settings.

substituent (right hand end of Fig. 8). The amine-substituent ring systems of compounds **24**–**26** and **36** are quite planar and are able to be accommodated between the negative steric regions. Whereas the non-planar tetrahydropyran ring system of compounds **14**–**19**, **21**–**23**, **29**–**35** all interact with the negative steric regions. Such interactions may explain why a low β_1-AR binding affinity is observed for many of the tetrahydropyran compounds.

The primary features of the CoMFA contour map for antagonist potency at the rat β_1-AR (Fig. 9) resemble the human map in that there are bulk preferring and negative steric regions at both ends of the contour map but the size varies somewhat. In particular, the

negative steric (yellow) region located near the *para*-position of the phenyl ring (left hand end of Figs. 8 and 9) is larger in the rat CoMFA contour map. The cyclopropyl ring of compound **32** interacts with this negative steric region in both the human and, to a greater extent, the rat contour maps. This steric interaction may explain why the rat CoMFA model predicts compound **32** to have such a low potency. The location and size of the negative electrostatic charge preferring (red) regions differ somewhat between the rat and human CoMFA maps (Figs. 8 and 9) and the rat β_1-AR map possesses an additional bulk preferring region adjacent to the

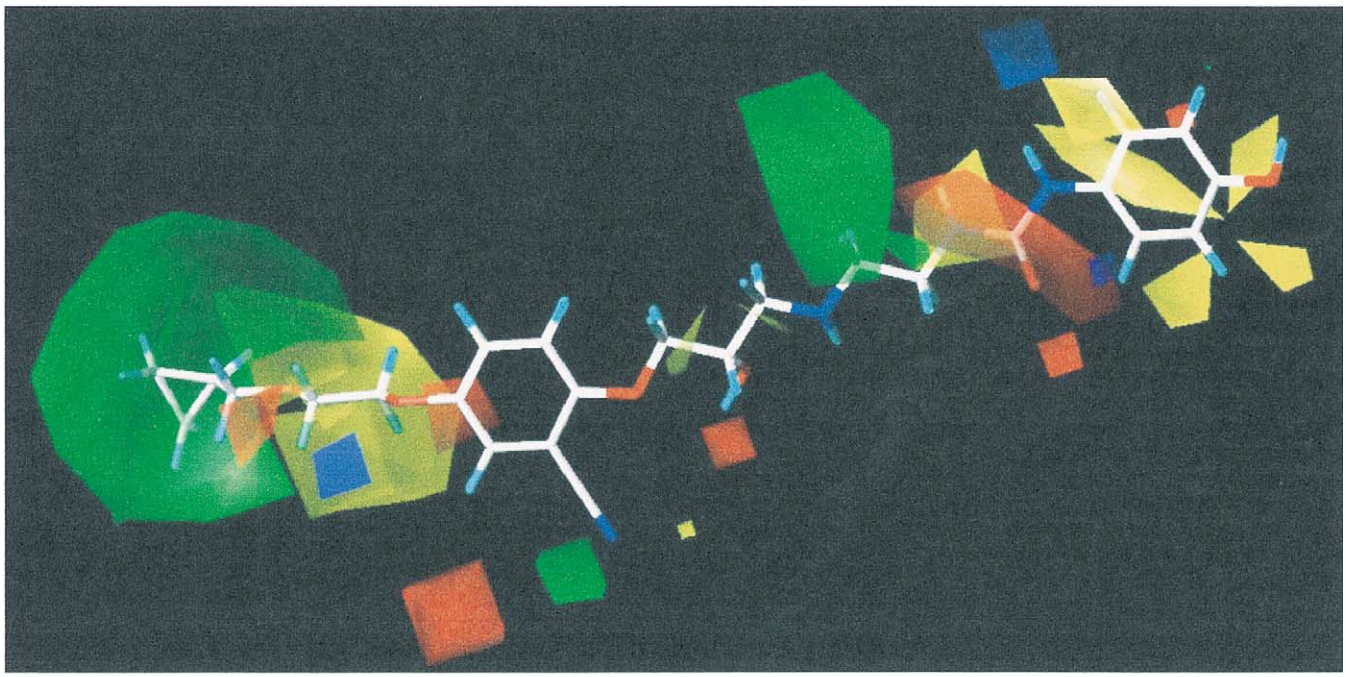

(a)

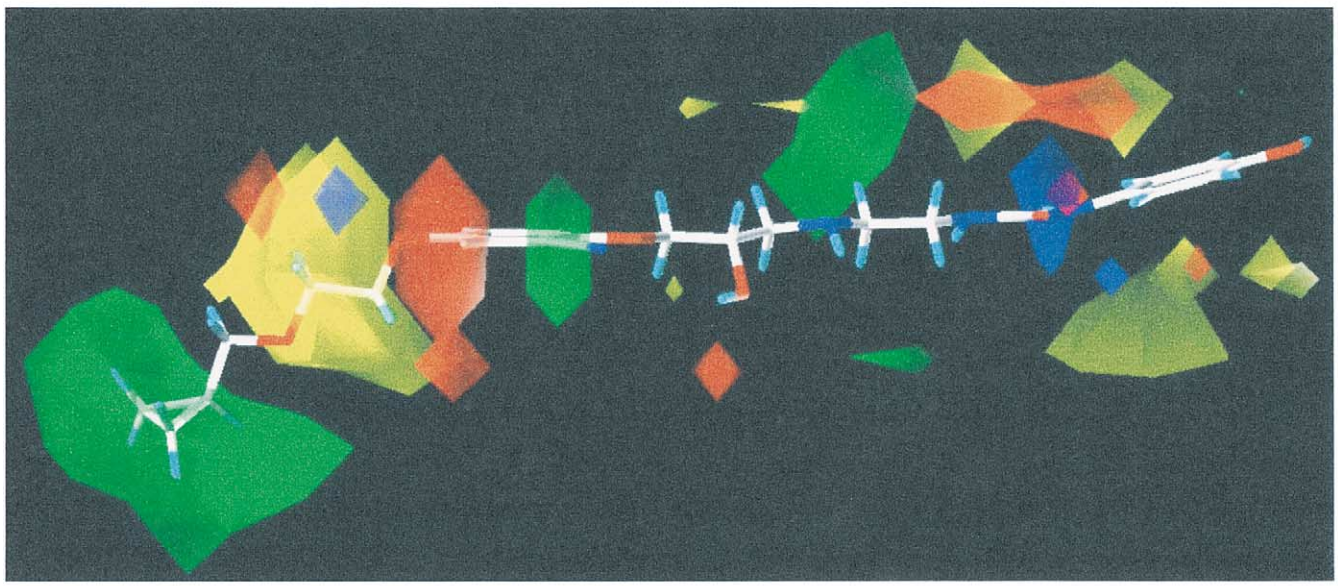

(b)

Fig. 9. Contour map of the final rat β_1-AR CoMFA model ($n = 32$) with compound **26** embedded, generated using the CoMFA steric and electrostatic fields. Green regions show favoured areas where increasing bulk is associated with higher binding affinity, yellow regions where increasing bulk is associated with lower binding affinity, blue regions where positive electrostatic charge is associated with higher binding affinity and red regions where negative electrostatic charge is associated with higher binding affinity: (a) view from above the phenyl ring; and (b) side view (i.e. 90° rotation about *x*-axis from view (a)). Transparent contours were drawn at the 70/30 level, all other 'view CoMFA' parameters were the default settings.

ortho-position of the phenoxypropanolamine phenyl ring. Compounds **10**–**14**, **20**, **26**, **30** and **33** all have substituents, which can access this additional bulk preferring region. The presence of this site in the rat map does not result in obvious differences in binding between the two species, suggesting that it may not be a major binding site. In fact, if we draw the CoMFA steric contours at 80 (instead of 70 as in Figs. 8 and 9) this additional bulk preferring region disappears and the steric rat CoMFA map more clearly resembles that of the human. The keto oxygen atom of compound **13** is also very close to the negative electrostatic charge (red) preferring region located in this area of the rat β_1-AR CoMFA map. The presence of negative steric (yellow) regions located near the *para*-position of the phenyl ring (left hand end of Fig. 9) and a bulk preferring pocket (green region) located after the negative steric region are consistent with the steric contour map from our previous CoMFA study of *N*-isopropylphenoxypropanolamines and rat β_1-AR pA_2 data [5].

6. Discussion

This work confirms and extends our previous observations on *para*-substituted *N*-isopropylphenoxypropanolamines [5] and describes the effects of *t*-butyl and longer amine-substituents on affinity to human as well as rat β_1-ARs. The major aim of this study was to investigate the structural requirements of phenoxypropanolamines to maximise antagonist binding to human β_1-ARs. This work differed from our earlier studies where the data was derived from in vitro functional studies in rat isolated atria and which only examined the effects of *para*-substitution upon antagonist potency. On this occasion, studies were conducted examining the binding affinity of the compounds for human β_1-ARs expressed in CHO cells and a much wider range of compounds was utilised including various *ortho*-, *meta*-, *para*- and amine-substitutions of a phenoxypropanolamine core structure. The advantages of the inhibition binding experiments over the functional studies are twofold in that they provide a better understanding of the structure–activity relationships of the target species, man, and significantly reduced the variability of the experimentally determined binding affinities. Functional studies in the rat were also carried out to allow comparison with the earlier data [5].

Compounds **1**, **4**–**9**, **27** and **28** are *para*-substituted *N*-isopropyl compounds for which we previously reported the steric CoMFA fields in the rat β_1-AR [5], in this paper, we describe steric and electrostatic CoMFA models for human as well as rat β_1-ARs. The new human and rat data suggests that the steric CoMFA contours surrounding the phenoxypropanolamine *para*-substituent are similar to that described in our previous report [5], i.e. there is a region of space where structural bulk reduces binding affinity close to the *para*-position of the phenyl ring (yellow region) and that there is a bulk preferring pocket a little further out from this position that is accessed by longer *para*-substituents which restores affinity (green regions, Figs. 8 and 9). Compounds with a short *para*-substituent, for e.g. compounds **2**, **3**, **31** and **32**, are unable to reach the bulk preferring pocket and are located within the negative steric region. Hence they have a lower binding affinity for the human receptor and lower potency at the rat receptor than the unsubstituted compound **1**. Longer, more flexible *para*-substituents, for e.g. compounds **6**, **8**, **9**, **27** and **28** are able to access the bulk preferring pocket and their binding affinity (or potency) is restored to a value approaching that of the unsubstituted compound **1**. Propranolol compound **10**, which has a napthyl ring system rather than a phenyl ring, also has high affinity for the β_1-AR and in the rat CoMFA map this can be explained by a steric binding site in the *ortho*/*meta* region of the phenoxypropanolamine structure. However, in the human CoMFA map this steric binding site does not appear to be present, suggesting that we may need to look at more compounds with substituents in this area to further resolve the CoMFA map. As indicated above, in our previous study [5] the electrostatic field was filtered out and the effect of *para*-substitution on β_1- and β_2-ARs was explained solely in terms of the steric CoMFA maps. In this study, we have also examined the electrostatic fields for both the human and rat β_1-AR and they show the presence of a positive electrostatic charge preferring region (blue) in close proximity to the amide functional group in the *para*-substituents of compounds **2**, **3** and **31** and negative electrostatic charge preferring regions (red) close to the oxygen atoms present in many of the *para*-substituents. The location of the negative electrostatic charge preferring regions in the CoMFA maps differs between the two species, however at this stage it is unclear whether this is due to structural differences in the human and rat antagonist binding sites.

The CoMFA maps for the human and rat β_1-ARs also provide information on potential interactions of the amine-substituent for these *N*-alkylphenoxypropanolamines. Both maps have similar features at the right hand end; they contain a bulk preferring region (green) which may be accessed by an appropriate α-substitution on the amine-substituent and a negative steric region (yellow) which reduces the binding affinity of the tetrahydropyran compounds. Compounds **12** and **13** have a *t*-butyl substituent, which can access the bulk preferring region in both CoMFA maps, which probably accounts for their increased affinity over compound **1**. Compounds **14**–**19**, **21**–**23** and **29**–**35** are all tetrahydropyran compounds. Comparison of the non-*para*-substituted compounds **1** and **29** indicates that

replacing a simple isopropyl amine-substituent with a larger substituent terminating with a tetrahydropyran ring decreases affinity by ca. 0.8 log units. Presumably, the tetrahydropyran occupies the negative steric region present in the CoMFA maps. Similar falls in affinity or potency occur when the *para*-substituted compounds **2**, **4**, **6**, **7**, **8** and **9** are compared with their tetrahydropyran analogs **31**, **15**, **16**, **17**, **19** and **21**, respectively. Increasing the length of the amine-substituent further increases contact with the negative steric region and thus further decreases the affinity for β_1-ARs in this series, compare compounds **19** and **22**. By contrast, amine-substituents terminating in a planar ring system (**24**–**26** and **36**) can be accommodated in both the human and rat CoMFA maps (Figs. 8 and 9). Such compounds avoid the negative steric regions (located at the right hand end of Figs. 8 and 9), thereby increasing the affinity for the β_1-AR and an example of this is shown by the effect of changing the amide tetrahydropyran in compound **34** to a urea indole in compound **36** with an increase in affinity of 1.7 log units.

The initial human β_1-AR CoMFA model predicted the experimental human β_1-AR binding affinities of the training set with low residual values (Table 4), a q^2 of 0.59 and an r^2 of 0.98. The model also predicted seven out of ten compounds in the test set with residual values ≤ 0.50 (Table 5, Fig. 6b). Of the three remaining compounds in the test set with residuals > 0.5 (compounds **27**, **28** and **32**), the difference between the experimental and predicted value was still less than 20%. The initial rat β_1-AR CoMFA model predicted five out of six test compounds with residuals ≤ 0.50 (Table 7, Fig. 7b). The rat model significantly underestimated (1.79 log units or 25%) the pA_2 value for compound **32**. Upon inspection of the rat CoMFA contour map it was found that the cyclopropyl ring of the *para*-substituent lay embedded within the negative steric region located at the left hand end of Fig. 9. Manual manipulation of only the torsion angle adjacent to the cyclopropyl ring of the *para*-substituent reduced the interaction of the cyclopropyl ring with the negative steric region. Therefore, in the rat CoMFA model it would appear that the current *para*-substituent conformation is not optimum for compound **32** and that the model predicts the potency to be much lower than the experimental value.

In summary, the steric and electrostatic CoMFA field parameters appear to be sufficient in explaining the binding affinity of this series of phenoxypropanolamines to both the human and rat β_1-AR. Furthermore, the CoMFA contour map from the present study provides a greater understanding of phenoxypropanolamine structure–activity relationships for human β_1-ARs. For instance, not only are bulk preferring pockets in the *para*-position of the phenyl ring identified (Fig. 8), but also short bulky substitutions close to the amine may increase binding affinity for example replacement of isopropyl with *t*-butyl (compounds **12** and **13**). They also provide an explanation for the lower binding affinity of the tetrahydropyran compounds (compounds **14**–**19**, **21**–**23**, **29**–**35**). So far we have only examined an extended low energy *N*-alkyl phenoxypropanolamine conformation. For the human β_1-AR we obtained a CoMFA model that will be useful in the design of new β_1-AR antagonists. However, although the rat β_1-AR CoMFA model predicted the small test set extremely well, the low q^2 value suggests the conformation chosen for our study may not be optimum and identifies the need to look at other feasible antagonist conformations.

7. Experimental

7.1. Materials

Compound **10** (propranolol) was purchased from Sigma Chemical Co. (St. Louis, MO, USA) and compounds **13** and **24** (CGP 12177 and CGP 20712A) from Research Biochemicals International (Natick, MA, USA). The following compounds were kindly donated: compound **11** (ICI-118,551) from ICI Pharmaceuticals (UK) and compound **7** (H87/07) from Astra Pharmaceuticals (Brussels, Belgium). Cyanopindolol (MH-C-706, Lot No. MF-I-44) was provided by Research Biochemicals International as part of the Chemical Synthesis Program of the U.S. National Institute of Mental Health, Contract N01MH30003. Cyanopindolol was radioiodinated by David Casley, Department of Medicine, The University of Melbourne using radioactive NaI and chloramine-T to produce ICYP.

7.2. Pharmacological methods

7.2.1. Radioligand binding studies

A CHO cell line transfected with human β_1-ARs was kindly provided by the Institut Cochin de Génétique Moléculaire, Paris, France. Binding studies with CHO cell membranes were conducted as described by Blin et al. [29]. Preconfluent cells were washed twice with ice-cold phosphate buffer and harvested with 25 mM Tris–HCl, pH 7.5, 1 mM EDTA buffer. Harvested cells were centrifuged at $10{,}000 \times g$ for 15 min and pellets were resuspended in Tris–HCl-EDTA homogenisation buffer and stored at -80 °C until needed.

Cells were thawed as required and suspended in Hank's balanced salt solution supplemented with 1 mM ascorbic acid, pH 7.4 at 200–500 μg protein ml^{-1} for all studies. Aliquots of cells were incubated with 200 pM ICYP in the absence or presence of competitor, in a 200 μl final volume of buffer, for 45 min at 37 °C in the dark and non-specific binding was determined in

the presence of 2 μM (±)-propranolol as described by Blin et al. [29]. Incubations were terminated by rapid filtration onto GF/C Whatman glass fibre filters presoaked with 0.01% polyethyleneimine and washing with 4×5 mL ice-cold phosphate buffer (pH 7.4). Filter-bound radioactivity was counted for 1 min using an LKB Multigamma counter.

Binding data were analysed using the iterative curve fitting programs EBDA Version 4.0 which incorporates LIGAND Version 4.0. The log of the inhibition constant (pK_i) (drug inhibition studies), dissociation constants (K_d) and binding density (B_{max}) values are shown as mean ± S.E.M. of individual analyses of binding isotherms using LIGAND. Pseudo Hill coefficients (n_H) were obtained from analysis of binding data using the sigmoidal fit of the EBDA program. Values represent mean ± S.E.M. of 3–9 individual experiments.

7.2.2. Rat isolated spontaneously beating atria

Studies were carried out on Sprague–Dawley rat isolated atria as described previously [5]. All tissues were allowed to equilibrate for 45 min with Krebs Ringer physiological salt solution; the composition of which in mmol L^{-1} was NaCl, 120; KCl, 5.6; $MgSO_4$, 1.2; $CaCl_2$, 2.5; KH_2PO_4, 1.4; $NaHCO_3$, 25; glucose, 11.2 and EGTA, 0.0025.

Cumulative concentration–response curves were obtained for the non-selective β-AR agonist (−)-isoprenaline in each preparation [5]. (−)-Isoprenaline was dissolved and diluted in 1 mg mL^{-1} ascorbic acid to prevent oxidation. For the measurement of antagonist activity, the appropriate agent was added to the organ bath at least 30 min after the first control concentration–response curve was completed and allowed to equilibrate for 10 min before the next concentration–response curve established. The pA_2 value was calculated from the shift in this curve to the right [30]. At least three concentrations of each antagonist were examined to verify the pA_2.

Rat hearts were removed from adult animals (200–250 g) and placed in Krebs Ringer salt solution (pH 7.4) aerated with 5% CO_2 in O_2. The atria were dissected free of the ventricles and overlying tissue and placed in a 20 mL bath maintained at 37 °C and connected to an isotonic transducer. A tension of 1 g was applied and chronotropic activity was amplified and recorded on a Grass Polygraph.

Acknowledgements

Cyanopindolol was provided by Research Biochemicals International as part of the Chemical Synthesis Program of the U.S. National Institute of Mental Health, Contract N01MH30003. The authors would like to thank David Casley (University of Melbourne) for the radioiodination of cyanopindolol, Professor A.D. Strosberg (Institut Cochin de Genetique Moleculaire, Paris) for providing the CHO cell line transfected with the human β_1-AR and Dr Margaret Wong (Department of Applied Chemistry, Swinburne University of Technology, Hawthorn, Victoria, Australia) for the use of the program PALLAS PROLOGP. SNL is supported by a National Health and Medical Research Council of Australia, INSERM Fellowship. This work was supported in part by grants from the National Health and Medical Research Council of Australia and the Austin Hospital Medical Research Foundation.

References

[1] J.M. Cruickshank, B.N.C. Pritchard (Eds.), Beta-Blockers in Clinical Practice, Churchill Livingstone, London, 1988.
[2] L.J. Emorine, S. Marullo, M.-M. Briend-Sutren, G. Patey, K. Tate, C. Delavier-Klutchko, D. Strosberg, Science 245 (1989) 1118–1121.
[3] T.J. Frielle, S. Collins, K.W. Daniel, M.G. Caron, R.J. Lefkowitz, B.K. Kobilka, Proc. Natl. Acad. Sci. USA 84 (1987) 7920–7924.
[4] B.K. Kobilka, R.A.F. Dixon, T. Frielle, H.G. Dohlman, M.A. Bolanowski, I.S. Sigal, T.L. Yang-Feng, U. Franke, M.G. Caron, R.J. Lefkowitz, Proc. Natl. Acad. Sci. USA 84 (1987) 46–50.
[5] S.N. Louis, T.L. Nero, D. Iakovidis, F.M. Colagrande, G.P. Jackman, W.J. Louis, Eur. J. Med. Chem. 34 (1999) 919–937.
[6] A.H. Beckett, Fortschr. Arzneim. Forsch. 1 (1959) 455–530.
[7] L.H. Easson, E. Stedman, Biochem. J. 27 (1933) 1257–1266.
[8] T.L. Nero, W.J. Louis, D. Iakovidis, J. Mol. Struct. (Theochem.) 285 (1993) 251–272.
[9] Kunz W., Jacobi H., Koch K., Geus R., GB Patent 1,147,032 (1969).
[10] Berthold R., Louis W.J., Stoll A., U.S. Patent 4,661,513 (1987).
[11] Louis W.J., Berthold R., Stoll A., U.S. Patent 4,970,238 (1990).
[12] Berthold R., Louis W.J., U.S. Patent 4,425,362 (1984).
[13] Louis W.J., Berthold R., Seiler M.-P., Stoll A., U.S. Patent 4,977,153 (1990).
[14] G.A. McPherson, Comput. Programs Biomed. 17 (1983) 107–113.
[15] P.J. Munson, D. Rodbard, Anal. Biochem. 109 (1980) 220–239.
[16] S.N.S. Louis, T.L. Nero, D. Iakovidis, G.P. Jackman, W.J. Louis, Eur. J. Pharmacol. 367 (1999) 431–435.
[17] J.M. Van Rossum, J.A.Th.M. Hurkmans, C.J.J. Wolters, Arch. Int. Pharmacody. Therap. 143 (1963) 299–330.
[18] B.R. Zaborowsky, W.C. McMahan, W.A. Griffin, F.H. Norris, R.R. Ruffolo Jr., J. Pharmacol. Meth. 4 (1980) 165–178.
[19] T.L. Nero, D. Iakovidis, W.J. Louis, in: F. Sanz, J. Giraldo, F. Manaut (Eds.), QSAR and Molecular Modelling: Concepts, Computational Tools and Biological Applications, Prous Science Publishers, S.A. Barcelona, Spain, 1995, pp. 528–530.
[20] J.B. Ball, T.L. Nero, D. Iakovidis, L. Tung, G. Jackman, W.J. Louis, J. Med. Chem. 35 (1992) 4676–4682.
[21] X.Q. Lewell, Drug Des. Discov. 9 (1992) 29–48.
[22] M.J.S. Dewar, E.G. Zoebisch, E.F. Healy, J.J.P. Stewart, J. Am. Chem. Soc. 107 (1985) 3902–3909.
[23] R.D. Cramer, D.E. Paterson, J.D. Bunce, J. Am. Chem. Soc. 110 (1988) 5959–5967.
[24] B. Belleau, Ann. N.Y. Acad. Sci. 139 (1967) 580–605.
[25] D.J. Triggle, in: D.J. Triggle, C.R. Triggle (Eds.), Chemical Pharmacology of the Synapse, Academic Press, London, 1976, p. 233.

[26] R.A.F. Dixon, I.S. Sigal, C.D. Strader, Cold Spring Harbor Symp. Quant. Biol. 3 (1988) 487–497.
[27] C.D. Strader, I.S. Sigal, R.B. Register, M.R. Candelore, E. Rands, W.S. Hill, R.A.F. Dixon, Proc. Natl. Acad. Sci. USA 84 (1988) 4384–4388.
[28] K. Wieland, H.M. Zuurmond, C. Krasel, A.P. Ijzerman, M.J. Lohse, Proc. Natl. Acad. Sci. USA 93 (1996) 9276–9281.
[29] N. Blin, L. Camoin, B. Maigret, A.D. Strosberg, Mol. Pharmacol. 44 (1993) 1094–1104.
[30] D. Mackay, J. Pharm. Pharmacol. 30 (1978) 312–313.